

Model and Deep learning based Dynamic Range Compression Inversion

Haoran Sun, Dominique Fourer and Hichem Maaref

November 8, 2024

Abstract

Dynamic Range Compression (DRC) is a popular audio effect used to control the dynamic range of a signal. Inverting DRC can also help to restore the original dynamics to produce new mixes and/or to improve the overall quality of the audio signal. Since, state-of-the-art DRC inversion techniques either ignore parameters or require precise parameters that are difficult to estimate, we fill the gap by combining a model-based approach with neural networks for DRC inversion. To this end, depending on the scenario, we use different neural networks to estimate DRC parameters. Then, a model-based inversion is completed to restore the original audio signal. Our experimental results show the effectiveness and robustness of the proposed method in comparison to several state-of-the-art methods, when applied on two music datasets.

1 Introduction

Dynamic Range Compression (DRC) is a fundamental process in audio signal processing which aims at changing the dynamic range of a signal. This technique is widely used in various stages of audio production, such as recording, mixing, and mastering, to control the loudness of an audio signal and prevent clipping or distortion [1]. However, the application of DRC often leads to changes in the audio’s timbre and perceived quality, making its inversion a challenging task. Thus, inverting DRC is full of interest in the context of audio reverse engineering [2] since it aims at recovering the original dynamic range and audio quality of a signal. This task could find many applications such as signal restoration, remixing, and enhancing creative control.

Inverting DRC is a challenging problem which often requires side information with an explicit DRC model and prior knowledge about the DRC parameters to be efficiently processed. There only exist a few studies which directly address the problem of DRC inversion. In [3], the authors consider DRC inversion as a rate-distortion optimization problem using a coder-decoder framework which minimizes both the side-information and the reconstruction error when combined with a specific estimator applied to the compressed signal. In [4], the authors propose a specific DRC model which provides promising reconstruction approximation but require to know exactly the DRC parameters of the compressed signal. Other work such as [5] only attempts to cancel or

to reduce the effects of DRC without directly addressing the challenging problem of inversion. More recent inversion methods based on deep learning only consider a specific type of DRC (eg. limiter, distortion, clip) and require for each of them a specific training dataset [6, 7].

In the present work, we propose to revisit the DRC inversion problem by resorting to deep neural network through a new approach which first identifies the mixture configuration to obtain the DRC parameters, and then applies the adequate model-based inversion to restore the original uncompressed signal. Our contributions are manifold. First, we propose a novel technique based on deep learning models which blindly predicts the DRC profile or parameters applied to an audio signal by analyzing the waveform of the compressed signal y . Second, we propose to use the estimated parameters corresponding to the predicted profile with a modified existing model-based DRC inversion technique first proposed by [4] to restore the original signal x . Finally we compare our proposal with several state-of-the-art methods applied on two public datasets in terms of parameter estimation accuracy, and signal reconstruction quality.

Our paper is organized as follows. Section 2 introduces the DRC inversion problem and describes our new approach, including signal processing and model design. Section 3 presents the experimental setup. Section 4 presents the numerical results of these experiments. Finally, Section 5 contains our conclusions and future work.

2 Methodology

2.1 Problem Statement

Let x be a one-dimensional real-valued discrete-time signal obtained at sampling rate F_s . We denote $x[n]$, $\forall n \in \{0, 1, \dots, N-1\}$ the n -th signal sample of the signal.

Now, we consider g , the gain function of the DRC effect applied to x for obtaining the compressed signal as:

$$y[n] = x[n] \cdot g_{x,q_\theta}[n], \quad (1)$$

The value of $g[n]$ depends on the signal x itself and the DRC parameters $q_\theta \in \mathbb{R}^7$, which is a set of parameters related to the compressor model $\theta \in \{0, 1, \dots, d-1\}$ is the label of a DRC profile, with d the maximum number of considered profiles.

Hence, this paper addresses the problem of blindly computing the estimates \hat{q}_θ and \hat{x} , which are the more close as possible from q_θ and x (in the minimum mean-squared error sense). We consider as unique observation, the compressed signal y and we assume that the applied DRC effect can be approximated using the proposed generic DRC model for which the parameters q are unknown.

2.2 Dynamic Range Compression

The reversible DRC model proposed in [4] enables to consider a large variety of compressor types (eg. expander, compressor, or noise gate, etc.) and uses the following set of parameters (cf. Table 1 for a description) $q_\theta = \{L, R, \tau_v^{\text{att}}, \tau_v^{\text{rel}}, \tau_g^{\text{att}}, \tau_g^{\text{rel}}, p\}$, where

- L : the threshold expressed in dB,

- R : the compression ratio,
- $\tau_v^{\text{att}}, \tau_v^{\text{rel}}$: the attack and release time (expressed in seconds), used to smooth the detection envelope,
- $\tau_g^{\text{att}}, \tau_g^{\text{rel}}$: the attack and release time (expressed in seconds), used to smooth the gain function,
- p : the compressor detection type (1: peak, 2: Root Mean Square).

The computation of g_{x,q_θ} is completed as follows. First, the detection envelope v is obtained from $x, p, \tau_v^{\text{att}}, \tau_v^{\text{rel}}$ as:

$$v[n] = \sqrt[p]{\beta|x[n]|^p + \bar{\beta}v[n-1]^p}, \quad \text{with } \bar{\beta} = 1 - \beta \quad (2)$$

with $\beta = 1 - e^{-\frac{2.2}{F_s \tau_v}}$, and $\tau_v = \begin{cases} \tau_v^{\text{att}} & \text{if } |x[n]| > v[n-1] \\ \tau_v^{\text{rel}} & \text{otherwise} \end{cases}$. Second, we compute the compression factor f using v and R as:

$$f[n] = \begin{cases} \left(\frac{l}{v[n]}\right)^{1-\frac{1}{R}} & \text{if } v[n] > l, \text{ with } l = 10^{L/20} \\ 1 & \text{otherwise} \end{cases} \quad (3)$$

Finally, the DRC gain g_{x,q_θ} is obtained by smoothing the compression factor f using τ_g^{att} and τ_g^{rel} such as:

$$g[n] = \gamma f[n] + (1 - \gamma)g[n-1] \quad (4)$$

with $\gamma = 1 - e^{-\frac{2.2}{F_s \tau_g}}$ and $\tau_g = \begin{cases} \tau_g^{\text{att}} & \text{if } f[n] > g[n-1] \\ \tau_g^{\text{rel}} & \text{otherwise} \end{cases}$. The compressed signal

is thus obtained using Equation 1. This process corresponds to the implementation included in many existing popular audio software such as SoX¹.

2.3 DRC Inversion using Known Parameters

The model presented in Section 2.2 allows to estimate \hat{x} from y when q_θ is exactly known. The overall method can be summarized in Algorithm 1 where $\kappa = l^S$ and $S = 1 - \frac{1}{R}$.

In [4], the author defined a CHARFZERO() function to estimate a zero-crossing values v_0 of the characteristic function based on the Newton-Raphson method, $\xi_p(v) =$

$$(\gamma \kappa v[n]^{-S} + \bar{\gamma} g[n-1]^p)(v[n]^p - \bar{\beta} v[n-1]^p) - \beta |y[n]|^p. \quad (5)$$

This function offers more control and flexibility, which can be useful for custom behavior and specific requirements in the root-finding process. However, this comes at the cost of increased complexity and the need for thorough testing. In this work, we replace the original CHARFZERO function with a modification of the Powell hybrid

¹SoX Sound eXchange <https://sox.sourceforge.net>

method as implemented in MINPACK [8], refereed as “root” function in the following. This function provides a more standardized and more optimized root-finding algorithm, according to our comparative results in Section 4.

Equation 5 can be used to obtain relevant information about the envelope of $v[n]$. Hence, when $v[n]$ is known, using $\tilde{x}[n] = v[n]^p$, we can deduce:

$$|x[n]| = \sqrt[p]{\tilde{x}[n] - \frac{1-\beta}{\beta}\tilde{x}[n-1]} \quad (6)$$

which enables the estimation of the instantaneous gain required to invert DRC: $g[n] = \frac{|y[n]|}{|x[n]|}$.

Algorithm 1: Pseudo-code of the DRC Inversion algorithm.

```

Function DRC inversion( $y, q_\theta$ )
     $\tilde{x}[n] \leftarrow 0, \quad g[n] \leftarrow 1, \forall n \in [0, N-1]$ 
    for  $n = 0$  to  $N-1$  do
        if  $|y[n]| > \sqrt[p]{\tilde{x}[n]} \cdot g[n]$  then
             $\beta \leftarrow 1 - e^{-\frac{2.2}{F_s \tau_{\text{att}}^v}}$ 
        else
             $\beta \leftarrow 1 - e^{-\frac{2.2}{F_s \tau_{\text{att}}^v}}$ 
        end
        if  $|y[n]| > \sqrt[p]{\frac{1}{\beta} \left( \left( \frac{\kappa}{g[n]} \right)^{\frac{p}{S}} - \beta \tilde{x}[n] \right)} \cdot g[n]$  then
             $\gamma \leftarrow 1 - e^{-\frac{2.2}{F_s \tau_{\text{att}}^g}}$ 
        else
             $\gamma \leftarrow 1 - e^{-\frac{2.2}{F_s \tau_{\text{att}}^g}}$ 
        end
         $h_n \leftarrow \gamma + \gamma g[n]$ 
        if  $|y[n]| > \sqrt[p]{\frac{1}{\beta} (l^p - \beta \tilde{x}[n])} \cdot h_n$  then
             $v[n] \leftarrow \sqrt[p]{\beta (|y[n]|/h_n)^p + \beta \tilde{x}[n]}$ 
             $v_0 \leftarrow \text{CHARFZERO}(v[n])$ 
             $|x_n| \leftarrow \sqrt[p]{(v_0^p - \beta \tilde{x}[n])/\beta}$ 
             $\tilde{x}[n] \leftarrow v_0^p$ 
             $g[n] \leftarrow |y[n]|/|x_n|$ 
        else
             $g[n] \leftarrow h_n$ 
             $|x_n| \leftarrow |y[n]|/g[n]$ 
             $\tilde{x}[n] \leftarrow \beta |x_n|^p + \beta \tilde{x}[n]$ 
        end
         $\hat{x}[n] \leftarrow \text{sign}(y[n]) \cdot |x_n|$ 
    end
    return  $\hat{x}$ 
end

```

2.4 Deep learning based DRC parameters estimation

In this work, we use two method for DRC parameters estimation. In case of the possible compressor choice options is known, estimating the compressor profile (label) θ instead of directly estimating the DRC parameters often leads to more accurate inversion results. Because we can directly find the corresponding parameters q through θ . The classification of DRC profile θ can be regarded as an audio classification task, since the signal compressed by a same DRC profile can be regarded as one type. On the contrary, if we only have the compressed signal y , estimating DRC parameters p by regression task is the only option. This method can achieve the same goal, but generally with lower accuracy.

2.4.1 DRC profile classification

Early approaches predominantly employed spectral features, and statistical descriptors, combined with classical machine learning algorithms [9, 10]. While these methods provided interpretable results, they often struggled with capturing complex audio patterns effectively and required manual feature engineering. In contrast, deep learning methods, particularly Convolutional Neural Networks (CNN) [11] and Recurrent Neural Networks (RNN) [12], have gained prominence due to their ability to automatically learn hierarchical representations from raw audio waveform or spectrograms. Among deep learning-based audio classification methods, the Audio Spectrogram Transformer [13] (AST) has emerged as a powerful approach for capturing both temporal and spectral features of audio signals. In view of the excellent performance of transformer-based models in audio classification tasks in existing studies, we also choose this model in our work.

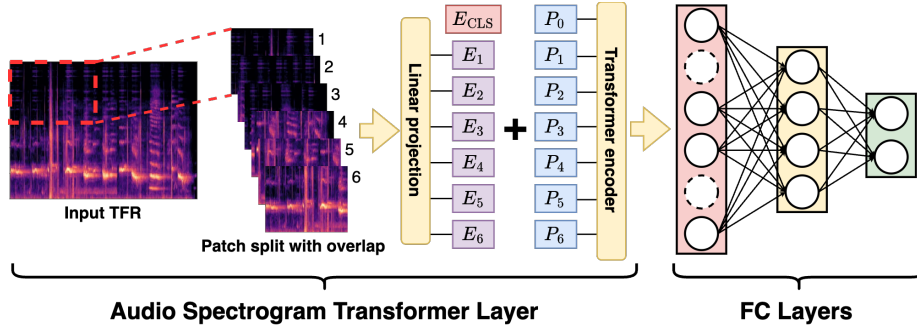


Figure 1: The architecture of the modified Audio Spectrogram Transformer (AST) model.

The architecture of the AST model is illustrated in Figure 1. First, the input audio signal y is transformed to a time frequency representation denoted TFR_y . In this work, we choose to use Mel Spectrum as this TFR_y . The detailed selection process is described in Section 4. Second, TFR_y is used as input of the proposed AST model. Thus, the TFR_y is split into a sequence of patches with an overlap in both time and

frequency dimension. Each patch is flattened to a 1D patch embedding E_i using a linear projection layer. Then a trainable positional embedding P_i is added to each patch embedding, allowing the model to capture the spatial structure of the 2D audio time-frequency representation. What’s more, a [CLS] token E_{CLS} is added at the beginning of the sequence as a classification label. Instead of the original model mapping the output of the transformer directly to an output layer with Sigmoid activation function, we use a MLP at the output. Each hidden layer is followed by a Batchnorm1d and a PReLU activation. The incorporation of additional fully connected layers enhances the model’s discriminative power, enabling it to capture subtle differences between different DRC profiles.

2.4.2 DRC parameters estimation

Although predicting the DRC profile can obtain accurate DRC parameters, directly estimating the DRC parameters is more general and will not be limited by the type of DRC profile. In the past, some studies have extended the use of early machine learning techniques to parameterize nonlinearities in physical models [14, 15]. Another computational intelligence approach [16] estimate synthesizer parameters using a multivariate linear regression model with hand-crafted features. More in line with the spirit of this paper is [17] on using U-Net to estimate parameters of multiple audio effects with the help of raw audio. In [18], 3 different encoders are used for audio effect parameters estimation. Among which, the Music Effect Encoder (MEE) [19] performed the best for compression task. In this work we use MEE for regressively estimate the DRC parameters. The architecture is illustrated in Figure 2.

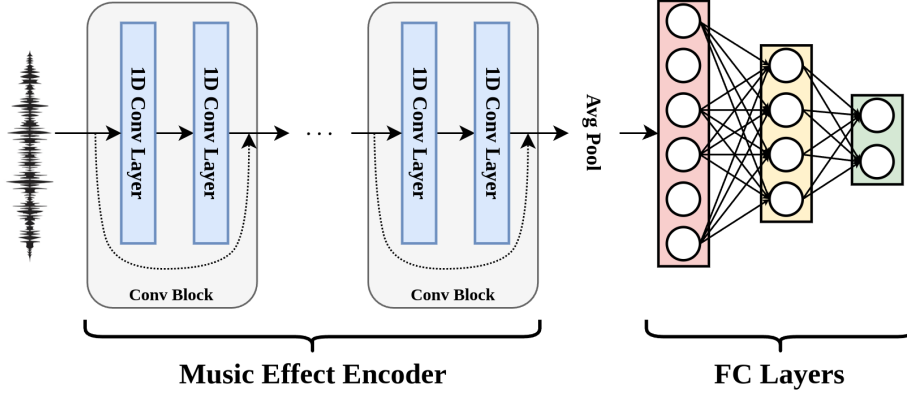


Figure 2: The architecture of the Music Effect Encoder.

The Music Effects Encoder consists of multiple 1-dimensional convolutional blocks, where each block includes two convolutional layers with a residual connection in between. Each convolutional layer is followed by a batch normalization and a rectified linear unit (ReLU) activation function. The output of the last convolutional layer is time-wise encoded through global average pooling, resulting in the dimensionality of 2048, and is used as the music effects feature. The music effect feature is mapped to

512-dimensional features using a linear layer for the contrastive objective, where the loss function used is normalized temperature-scaled cross-entropy loss. At the output, we use a MLP with 4 layers of size 2048, 1024, 512, and C where C is the total number of DRC parameters. Each hidden layer is followed by a Batchnorm1d and a PReLU activation. The output layer, which estimates normalized parameters, is followed by a sigmoid.

2.5 Overall Proposed Method

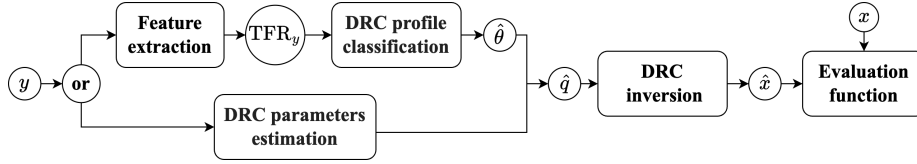


Figure 3: Proposed DRC inversion approach.

Now, we propose a new end-to-end DRC inversion method illustrated in Figure 3. It involves a two-phase approach, integrating deep learning techniques and the model-based inversion method presented in Section 2. Taking the compressed signal y as input, we either perform a classification task and use the AST model to predict the DRC profile $\hat{\theta}$; or perform a regression task and use the MEE model to estimate the DRC parameters \hat{p}_{θ} . Then, the DRC inversion model uses the compressed signals y and \hat{q}_{θ} to estimate the original signal \hat{x} .

3 Experiments

3.1 Datasets

In this work, we validate our model on two datasets: MedleyDB [20] with a sampling frequency of $F_s = 44,100$ Hz, and DAFX [21] with a sampling frequency of $F_s = 32,000$ Hz. Note that, the DAFX dataset provides raw music data, which can be directly used for signal compression and inversion. However, the MedleyDB dataset provides the raw tracks of various instruments and vocals, which should be mixed to obtain a raw music and then be compressed.

For the MedleyDB dataset, we randomly select 30 songs from the MedleyDB dataset with a total duration of about 1.6 hours and divide them into 5,785 segments of duration $t = 5s$. For DAFX dataset, for consistency, we extract the same number of music clips. Besides, to ensure effective compression, we delete the segments with a maximum Root Mean Square (RMS) peak less than $-60dB$. The results are our ground-truth original signal x .

To simulate dynamic range compression, we consider the five distinct DRC profiles in Table 1. These DRC profiles correspond to standard compressor presets proposed previously investigate in [4]. Each clip is compressed by these five compressors. As a result, we get two datasets corresponding to the compressed signal y , respectively

Parameter	Description	A	B	C	D	E
L (dBFS)	Threshold	-32	-19.9	-24.4	-26.3	-38.0
R (dB _{in} :dB _{out})	Ratio	3.0 : 1	1.8 : 1	3.2 : 1	7.3 : 1	4.9 : 1
τ_v^{att} (ms)	Envelope attack	5.0	5.0	5.0	5.0	5.0
τ_v^{rel} (ms)	Envelope release	5.0	5.0	5.0	5.0	5.0
τ_g^{att} (ms)	Gain attack	13.0	11.0	5.8	9.0	13.1
τ_g^{rel} (ms)	Gain release	435	49	112	705	257
p (1 or 2)	Detector type	2	2	2	2	2

Table 1: The selected DRC profiles for model exploration.

refereed as “M-6” and “D-6”. Each comprising a total of 6,942 clips categorized into six distinct classes based on the applied DRC profiles, as well as the neutral signal, labeled as “O”, which corresponds to raw signal where no compression is applied. The five aforementioned DRC profiles, are labeled as same as the DRC profile (“A”, “B”, “C”, “D” and “E”).

However, using a dataset containing only 6 signals makes the task too simple, and the trained model will be too restricted. So the above dataset is only used to explore the best settings of the model. To ensure the generality of the model, we also create two larger dataset using 30 DRC profiles. These 30 DRC profiles are generated according to the parameters range given in [1], as shown in the Table 2. Each range is equally divided into 30 equal intervals, and a value is randomly and without duplication selected from each range to form a profile.

Parameter	L (dB)	R	τ_v^{att} (ms)	τ_v^{rel} (ms)	τ_g^{att} (ms)	τ_g^{rel} (ms)	p
Range	[-60, -20]	[2, 15]	[5, 130]	[5, 130]	[25, 500]	[25, 2000]	2

Table 2: The selected DRC parameter ranges for model generalization.

As a result, we get two larger datasets, each contains 35,867 samples (≈ 49.8 h) of 31 classes of signal (30 DRC profiles + Neutral signal), respectively refereed as “M-31” and “D-31”. Once our model achieved good performance on the smaller datasets, we retrain the model using there larger datasets to verify the generality.

3.2 Experimental Settings

Hardware infrastructure features an Nvidia RTX 4080 GPU, and the software stack revolved around Python as the primary programming language and PyTorch as the deep learning framework of choice. Our evaluation workflow follows a standard supervised machine learning protocol, with the dataset partitioned into training and test sets using an 4 : 1 split ratio.

We uses an Adam optimizer with an initial learning rate of 10^{-4} and a batch size of 12 during a maximum of 500 epochs, decreasing the learning rate per epoch with the exponential way by a factor of $\alpha = 0.98$. Training stops after 50 epochs without

improvement. In our evaluation, we use the model weights from each configuration that achieved the lowest validation loss during training.

For the DRC profile classification task, we minimize the Cross Entropy Loss between the estimated labels and the real labels. Our evaluation considers standard classification metrics, including accuracy, precision, recall, and F1-score, computed from the confusion matrix obtained during testing. For the DRC parameters estimation task, we minimize the Mean Squared Error Loss between the estimated parameters and the real ones.

3.3 Training approaches

In order to make the results comparable, for the DRC inversion task, as illustrated in Figure 4, we compare 2 approaches for training:

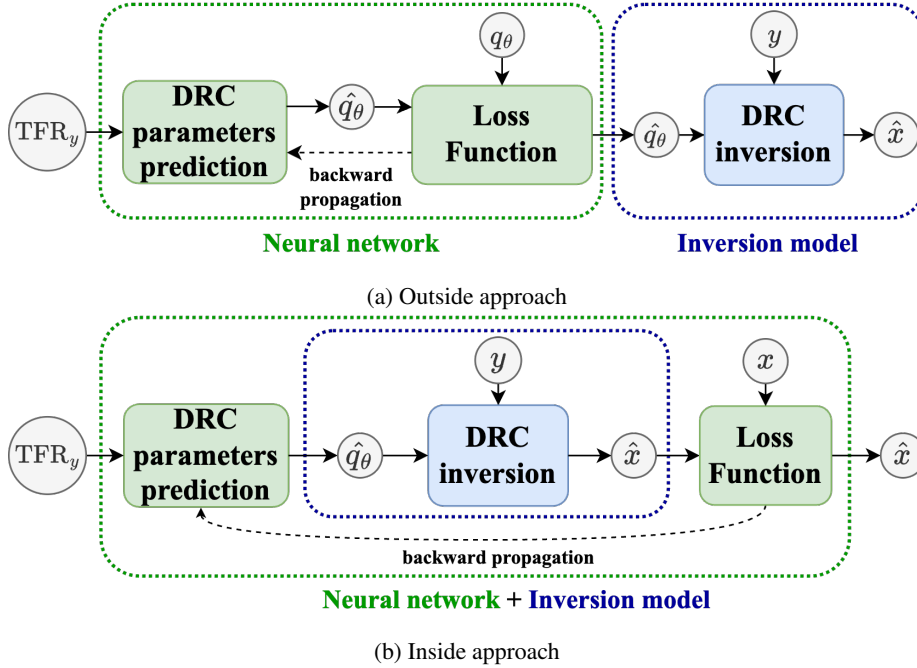


Figure 4: Two different approaches for training the classification model and inverting the DRC. The “Outside” approach corresponds to our proposal, the “Inside” approach serves as a comparison.

Outside approach: cf. Figure 4(a), the deep learning model and the inversion model do not interfere with each other. First, we train the neural network model for estimating the DRC parameters \hat{q}_θ . Thus, the estimated parameters \hat{q}_θ are used for the model-based inversion of y .

Inside approach: cf. Figure 4(b), the inversion model is integrated into the training process. Instead of predicting \hat{q}_θ , we use it to inverse DRC, and minimize the error

between the estimated signal \hat{x} and the real signal x .

In this work, we minimize the l^1 norm between the log-magnitude mel spectrogram of \hat{x} and x :

$$\mathcal{L}_{\hat{x},x}^{\text{Mel}} = \| \ln(|\text{Mel}_{\hat{x}}|) - \ln(|\text{Mel}_x|) \|_1 \quad (7)$$

in this case, the model outputs will be directly the estimated signal \hat{x} .

3.4 Evaluation

For evaluation, we compute the following metrics:

- $\mathcal{L}_{\hat{x},x}^{\text{MSE}}$: the Mean Square Error (MSE) between \hat{x} and x :

$$\mathcal{L}_{\hat{x},x}^{\text{MSE}} = \frac{1}{N} \sum_{n=0}^{N-1} (\hat{x}[n] - x[n])^2 \quad (8)$$

- $\mathcal{L}_{\hat{x},x}^{\text{Mel}}$ given by Equation 7

Both the original signal x and the estimated signal \hat{x} are normalized by their respective RMS values.

4 Numerical Results

Our experimental results are mainly divided into three parts: First, we show the algorithm optimization of the DRC model and discuss the possible reasons. Second, we show the results of the exploration experiment and the generality verification experiment of the AST and MEE models respectively. Finally, we give the DRC inversion results using the complete model and the comparison with some state-of-the-art models.

4.1 Algorithm optimization

We first show the optimization results of the CHARFZERO function in the DRC inversion model. A simple test to compare the performance of the two root-finding methods is made. The test audio is a music in MedleyDB dataset of duration $t = 57$ s. We first compress the music, and then decompress it using decompressors with different root-finding methods, then compare the decompression time and error. The used DRC profile is the profile “A” in Table 1.

As results, the decompression time of using the original CHARFZERO function is 260.3s, while that of using *root* function is 247.2s. Meanwhile, The $\mathcal{L}_{\hat{x},x}^{\text{MSE}}$ between the estimated signal \hat{x} and the original signal x is -62.18 dB for the original CHARFZERO function, while -73.69 dB for the alternative function.

Mathematically, *root* uses the Levenberg-Marquardt (LM) method, which is effective for nonlinear root-finding because it dynamically combines both gradient-descent and Gauss-Newton methods. For the nonlinear function $\xi_p(v) = 0$, LM minimizes: $\| \xi_p(v) \|^2$, and iteratively adjusts parameters to reduce both local error and sensitivity

to initial conditions. By dynamically adjusting step sizes and directions based on the curvature of $\xi_p(v)$, LM can converge faster and achieve high precision, especially near roots.

In terms of theoretical complexity, assuming ξ_p has a time complexity of $\mathcal{O}(1)$, CHARFZERO has a complexity of $\mathcal{O}(nX)$, where n is the number of iterations required for convergence and X is the time complexity of the ξ_p function. Meanwhile, *root* has an overall complexity typically estimated as $\mathcal{O}(nm)$, where m is the complexity of evaluating the function at each iteration, and n is minimized through adaptive methods. For typical nonlinear root-finding tasks, Root methods tend to reach optimal convergence rates in $\mathcal{O}(\log(1/\epsilon))$, leading to lower iteration counts n than simpler, non-adaptive methods.

4.2 Model exploration

4.2.1 DRC profile classification results

To the best of our knowledge, there is no study which propose to use AST for compressed audio signal classification, we first evaluate its performance for the DRC profile classification task. Thus, we conduct three comparative experiments to decide what is the best choice of input features, input TFR_t size, and the best neural network architecture.

Being inspired by [22], we empirically compare different TFR_y : namely Mel Frequency Cepstral Coefficients (MFCC), Short-Time Fourier Transform (STFT) spectrogram, Mel Spectrogram (Mel sp.) and Constant-Q Transform (CQT) spectrogram, and evaluate their impact on the classification performance of DRC profiles. All the time-frequency features are computed using *librosa* [23]. Table 3 presents the numerical results. In this experiment, the input size of each time-frequency representation is (128, 431). According to the accuracy, using Mel spectrogram as input TFR_y achieves the best classification results on both datasets. Specifically, on the MedleyDB dataset, the Mel sp. achieved an accuracy of 0.9558, while on the DAFX dataset, it achieved an accuracy of 0.9982. It is worth noting that the training time per epoch for Mel spectrogram is also relatively low, indicating its efficiency.

Dataset	Input	Time/epoch	Acc	Pre	Re-call	F1
MedleyDB	MFCC	0.15h	0.7869	0.7869	0.7869	0.7869
	STFT	0.12h	0.9418	0.9452	0.9418	0.9418
	Mel sp.	0.13h	0.9547	0.9590	0.9547	0.9547
	CQT	1.20h	0.7325	0.7325	0.7325	0.7325
DAFX	MFCC	0.15h	0.8963	0.9265	0.8963	0.8963
	STFT	0.12h	0.9794	0.9812	0.9794	0.9794
	Mel sp.	0.12h	0.9881	0.9904	0.9881	0.9881
	CQT	1.20h	0.8328	0.8328	0.8328	0.8328

Table 3: Comparison between training using different input TFR_y , with AST model for classification.

Although DRC is a time domain transform, it brings changes in both the time domain and frequency domain. Due to space limitations, we cannot present all experimental results. However, our preliminary experiments show that for the DRC profile classification task, the influence of time domain changes is greater than that of frequency domain changes. Therefore, we select some time-frequency feature sizes with larger time domain size and smaller frequency domain size as comparison objects. Table 4 presents the experimental results of varying sizes on the performance of the Mel spectrogram. For the MedleyDB dataset, the feature size of (64, 431) yielded the highest scores. The experiments with input sizes of (128, 431) also yielded favorable results. For the DAFX dataset, the feature size of (128, 431) and (128, 862) resulted in the best classification performance.

Dataset	Input size	Time/epoch	Acc	Pre	Re-call	F1
MedleyDB	(64, 431)	0.10h	0.9632	0.9741	0.9632	0.9632
	(128, 431)	0.12h	0.9555	0.9555	0.9555	0.9555
	(512, 431)	0.17h	0.9489	0.9505	0.9489	0.9486
	(128, 862)	0.11h	0.9582	0.9587	0.9582	0.9582
DAFX	(64, 431)	0.10h	0.9586	0.9586	0.9586	0.9586
	(128, 431)	0.12h	0.9881	0.9904	0.9881	0.9881
	(512, 431)	0.17h	0.9741	0.9749	0.9741	0.9741
	(128, 862)	0.11h	0.9877	0.9877	0.9877	0.9877

Table 4: Comparison between training using different input size of a Mel spectrogram, with the original AST model for classification.

Varying the number of fully connected (FC) layers in the AST model enables us to gauge its capacity to learn intricate patterns within Mel spectrogram. Specifically, we evaluate the use of 1, 2, and 3 FC layers. For MedleyDB, we use Mel spectrogram of size (64, 431) as input, while for DAFX, we use Mel spectrogram of size (128, 431). Table 5 presents the experimental results. For both the MedleyDB and DAFX dataset, varying the number of FC layers shows notable differences in classification performance. Employing a single FC layer yields competitive results, however, increasing the number of FC layers to two achieves the highest accuracy across both datasets, indicating the potential of deeper architectures in capturing intricate features for DRC profile classification. Nevertheless, further increasing the number of FC layers to three shows a slight decrease in performance, suggesting potential overfitting or the introduction of unnecessary complexity that hampers the model’s ability to generalize.

In summary, for the DRC profiles classification task, the best choice of input feature is (64, 431) Mel spectrogram for MedleyDB dataset, (128, 431) Mel spectrogram for DAFX dataset. Meanwhile, the best model architecture is the original AST model connected by 2 FC layers.

Table 6 shows the detailed validation results corresponding to the above two configurations. For both datasets, profiles C and E are well predicted. For neutral and profile B, the results drop slightly. For the MedleyDB dataset, profile A are occasionally misclassified as profile D, indicating potential overlap or similarity in acoustic features

Dataset	FC-layer	Time/epoch	Acc	Pre	Re-call	F1
MedleyDB	1 FC layer	0.10h	0.9632	0.9741	0.9632	0.9632
	2 FC layers	0.21h	0.9754	0.9754	0.9754	0.9754
	3 FC layers	0.23h	0.9412	0.9480	0.9412	0.9412
DAFX	1 FC layer	0.12h	0.9881	0.9904	0.9881	0.9881
	2 FC layers	0.20h	0.9952	0.9952	0.9952	0.9952
	3 FC layers	0.24h	0.9685	0.9685	0.9685	0.9685

Table 5: Comparison between training using different number of fully connected layers

that the model struggles to differentiate. Conversely, for the DAFX dataset, profile D are sometimes misclassified as profile A, indicating a different pattern of confusion compared to the MedleyDB dataset.

Combining Table 1 and Table 6, we try to analyze the reasons for misclassification. For Neutral and profile B, there are only a few cases of misclassification. According to the parameter values in profile B, we believe that the small value of compression ratio “R”, which may result in the signal compression amount being too little for some audio clips with a lot of white space, making it difficult to distinguish from uncompressed signals. For profiles A and D, their parameter values have in common that the gain release time $\tau_{g,rel}$ is very large. Given that DRC mainly reflects changes in the time domain, the slow gain release means that once the compression effect is applied, the input signal drops to the threshold. After this, it takes a lot of time for the gain to return to its original level. The slow recovery of gain causes the signal to continue to decay even after the input level is reduced, resulting in similar perceptual characteristics between the two profiles. Despite these differences, both confusion matrices highlight the model’s overall robustness in classification, with high accuracy and performance across most classes. These insights underscore the effectiveness of the model in audio signal processing tasks, while also identifying specific areas for potential improvement and refinement to enhance classification accuracy further.

Now, we retrain these models using the larger datasets “M-31” and “D-6” mentioned in Section 3, in order to reduce the limitations and explore the generality of our model. The experimental results are shown in Table 7.

4.2.2 DRC parameters estimation results

Unlike the AST model, there have been advanced studies using MEE model to estimate the parameters of the audio effect model [18]. Although it is not the same DRC model, their estimated parameters are also of dimension 6. Therefore, in this work, we directly use the same model configuration. In this task, we minimize the Mean Square Error of estimated parameters \hat{q}_θ and the real parameters q_θ :

$$\mathcal{L}_{\hat{q}_\theta, q_\theta}^{\text{MSE}} = \frac{1}{C} \sum_{i=0}^{C-1} (\hat{q}_\theta[i] - q_\theta[i])^2 \quad (9)$$

ref. class	Neutral	A	B	C	D	E
Neutral	220	0	8	0	0	0
A	0	209	0	0	22	0
B	3	0	227	1	0	0
C	0	0	0	245	0	0
D	0	18	0	0	209	0
E	0	0	0	0	0	227

(a) Confusion matrix of experiment using MedleyDB dataset, Mel spectrogram of size (64, 431).

ref. class	precision	recall	f1-score
Neutral	1.0000	0.9689	0.9821
A	0.9082	0.9133	0.9133
B	0.9774	1.0000	0.9825
C	1.0000	1.0000	1.0000
D	0.9212	0.9099	0.9212
E	1.0000	1.0000	1.0000
accuracy			0.9754
macro avg	0.9738	0.9738	0.9738
weighted avg	0.9754	0.9754	0.9754

(b) Evaluation metrics of experiment using MedleyDB dataset.

ref. class	Neutral	A	B	C	D	E
Neutral	217	0	2	0	0	0
A	0	191	0	0	5	0
B	2	0	233	0	0	0
C	0	0	0	241	0	0
D	0	6	0	0	230	0
E	0	0	0	0	0	262

(c) Confusion matrix of experiment using DAFX dataset, Mel spectrogram of size (128, 431).

ref. class	precision	recall	f1-score
Neutral	1.0000	0.9986	0.9986
A	0.9031	0.9845	0.9462
B	0.9878	1.00	0.9992
C	1.0000	1.0000	1.0000
D	0.9914	0.9178	0.9552
E	1.0000	1.0000	1.0000
accuracy			0.9952
macro avg	0.9951	0.9851	0.9951
weighted avg	0.9952	0.9952	0.9952

(d) Evaluation metrics of experiment using DAFX dataset

Table 6: Detailed results obtained using the two best experimental configurations.

Task	Accuracy	
	MedleyDB	DAFX
Exploration	0.9754	0.9952
Generalization	0.8509	0.8721

Table 7: DRC profiles classification results.

where C is the total number of DRC parameters. As the AST model, we first use the small datasets “M-6” and “D-6” to verify the performance of MEE model on DRC parameters estimation task, then test the model on the larger datasets for generalization. Table 8 shows the experimental results.

For the exploration results, the MEE model shows reasonable performance on both datasets, though with slightly lower $\mathcal{L}_{\hat{q}_\theta, q_\theta}^{\text{MSE}}$ and higher variability on the MedleyDB dataset. The results show that distinct audio properties could impact the encoder’s ability to generalize and the consistency of its estimates.

Task	$\mathcal{L}_{\hat{q}_\theta, q_\theta}^{\text{MSE}}$	
	MedleyDB	DAFX
Exploration	0.0235 ± 0.0228	0.0264 ± 0.0176
Generalization	0.0307 ± 0.0628	0.0343 ± 0.0597

Table 8: DRC parameters estimation results.

Combine the Table 7 and Table 8, we conclude that increasing the number of DRC profiles significantly reduces the accuracy of the classification task and increase the error of the regression task. Since the previous experiments using small datasets are too simple, the generalization experiments of the model greatly increased the complexity. We believe that the poor experimental results are reasonable and acceptable. Due to the nonlinearity and complexity of DRC, using different parameter settings may lead to the same variation results. Therefore, we recommend using the experimental results of model generalization and directly operating the DRC inversion.

4.3 DRC inversion results

On the premise that the results of the DRC profile classification experiment were good enough, we perform the DRC inversion experiment.

The classification results $\hat{\theta}$ or the regression results \hat{q}_θ , together with the compressed signal y are used as the input of the DRC inversion model, the total number of test samples for both “M-31” and “D-31” dataset is 7,173.

Table 9 shows the experimental results describing the average loss and the associated standard variation. For both the DRC profile task and the DRC parameter estimation task, the $\mathcal{L}_{\hat{x}, x}^{\text{MSE}}$ and $\mathcal{L}_{\hat{x}, x}^{\text{Mel}}$ loss of the “outside” inversion approach are lower than those of the “inside” inversion approach, for both datasets. This may be attributed to the direct integration of the inversion process into the neural network, since the esti-

Task	Approach	Dataset	$\mathcal{L}_{\hat{x},x}^{\text{MSE}}$	$\mathcal{L}_{\hat{x},x}^{\text{Mel}}$
Classification	Inside	M-31	0.075 ± 0.077	0.32 ± 0.14
		D-31	0.081 ± 0.090	0.32 ± 0.21
	Outside	M-31	0.0082 ± 0.0071	0.054 ± 0.043
		D-31	0.018 ± 0.026	0.076 ± 0.051
Regression	Inside	M-31	0.092 ± 0.104	0.25 ± 0.15
		D-31	0.089 ± 0.085	0.22 ± 0.26
	Outside	M-31	0.011 ± 0.014	0.082 ± 0.075
		D-31	0.023 ± 0.037	0.079 ± 0.082

Table 9: The experimental results depicting the average loss and associated standard variation of verification using samples from the test set following the inversion of DRC.

mated DRC profiles or parameters are not optimized, while our DRC inversion model requires precise parameters, which may lead to suboptimal reconstructions. While the “inside” method provides an integrated and potentially simplified process, it may come at the expense of poorer reconstruction quality compared to the “outside” method.

4.4 Baseline method comparison

At the end, we conduct a comparative experiment with baseline methods to further validate the effectiveness of our proposed model-based method. Demucs [24] is an advanced neural network-based model designed for music source separation tasks. In [25], the authors used Demucs to achieve removing distortion and clipping applied to guitar tracks for music production and got good results. In [7], the authors considered removing multiple audio effects from the same recording and proposed RemFX, a end-to-end approach that dynamically combines effect-specific removal models. These two pure neural network methods are selected as baseline methods. Besides, we also use the real parameters q to directly operate the DRC inversion as a reference for our proposed model, refereed as “Ref” in the table. Since the parameters are correct, the error given in this case should be minimal. In principle, the DRC inversion error of our method should be greater than that of the reference method.

Table 10 provides the comparative results of our proposed method with two baseline methods (Demucs and RemFX) for the task of DRC inversion across two datasets, MedleyD and DAFX. For the AST and MEE models, the experimental settings are exactly the same as the previous subsections. For the two baseline methods, we use the implementations provided by the original authors and retrain the models with our datasets “M-31” and “D-31”.

The results demonstrates that DRC profile classification based DRC inversion is the most effective method among the tested approaches, providing the lowest errors next to the reference. The regression approach is a viable alternative but exhibits slightly higher errors and variability. Meanwhile, our proposed methods provide show better performance compared to both the baseline methods in our experiments.

Model	Dataset	$\mathcal{L}_{\hat{x},x}^{\text{MSE}}$	$\mathcal{L}_{\hat{x},x}^{\text{Mel}}$
Ref	M-31	0.0052 ± 0.0049	0.023 ± 0.016
	D-31	0.0078 ± 0.026	0.056 ± 0.051
Classification	M-31	0.0082 ± 0.0071	0.054 ± 0.043
	D-31	0.018 ± 0.026	0.076 ± 0.051
Regression	M-31	0.011 ± 0.014	0.082 ± 0.075
	D-31	0.023 ± 0.037	0.079 ± 0.082
Demucs	M-31	0.27 ± 0.41	0.52 ± 0.42
	D-31	0.32 ± 0.19	0.59 ± 0.30
RemFX	M-31	0.027 ± 0.039	0.072 ± 0.063
	D-31	0.040 ± 0.027	0.094 ± 0.11

Table 10: DRC inversion task comparison between our model-based method and baseline methods.

5 Conclusion

In this paper, we have developed a model-based method coupled with deep learning techniques for DRC inversion, with a focus on inferring DRC profiles. Our promising results show the effectiveness of the proposed approach for reconstructing audio signals while simultaneously estimating the underlying DRC profiles. The proposed modified AST model obtained better results in DRC profile type classification and inversion accuracy compared to traditional audio classification methods presented in [26].

Our approach opens new avenues for improving audio quality, enabling finer creative control, and meeting industry demands for efficient audio processing tools. The ability to accurately infer DRC parameters offers opportunities for enhancing audio mastering, sound design, and audio restoration applications, ultimately enhancing the overall listening experience.

We acknowledge certain limitations and areas for improvement for our method. The model is only evaluated with compression and limiter but is not evaluated on expander and compander. Future research directions may involve exploring alternative parameter-based inversion model using neural network, and further numerical experiments considering other types of compressor.

6 Acknowledgement

This research was supported by the French ANR projects AQUA-RIUS (ANR-22-CE23-0022).

References

- [1] U. Zölzer, X. Amatriain, D. Arfib, J. Bonada, G. De Poli, P. Dutilleux, G. Evangelista, F. Keiler, A. Loscos, D. Rocchesso *et al.*, *DAFX-Digital audio effects*. John Wiley & Sons, 2002.
- [2] D. Barchiesi and J. Reiss, “Reverse engineering of a mix,” *Journal of the Audio Engineering Society*, pp. 563–576, 2010.
- [3] B. Lachaise and L. Daudet, “Inverting dynamics compression with minimal side information,” in *DAFx*, 2008.
- [4] S. Gorlow and J. D. Reiss, “Model-based inversion of dynamic range compression,” *IEEE Transactions on Audio, Speech, and Language Processing*, pp. 1434–1444, Jul. 2013.
- [5] K. Patel, *Acoustic Feedback Cancellation and Dynamic Range Compression for Hearing Aids and Its Real-Time Implementation*. The University of Texas at Dallas, 2020.
- [6] C.-B. Jeon and K. Lee, “Music de-limiter networks via sample-wise gain inversion,” in *IEEE WASPAA*, 2023, pp. 1–5.
- [7] M. Rice, C. J. Steinmetz, G. Fazekas, and J. D. Reiss, “General purpose audio effect removal,” in *IEEE WASPAA*, 2023, pp. 1–5.
- [8] J. J. Moré, B. S. Garbow, and K. E. Hillstom, “User guide for minpack-1,” CM-P00068642, Tech. Rep., 1980.
- [9] F. Rong, “Audio classification method based on machine learning,” in *ICITBS*, 2016, pp. 81–84.
- [10] L. Lu, H. Jiang, and H. Zhang, “A robust audio classification and segmentation method,” in *the ninth ACM international conference on Multimedia*, 2001, pp. 203–211.
- [11] S. Hershey, S. Chaudhuri, D. P. Ellis, J. F. Gemmeke, A. Jansen, R. C. Moore, M. Plakal, D. Platt, R. A. Saurous, B. Seybold *et al.*, “Cnn architectures for large-scale audio classification,” in *IEEE ICASSP*, 2017, pp. 131–135.
- [12] M. Scarpiniti, D. Comminiello, A. Uncini, and Y.-C. Lee, “Deep recurrent neural networks for audio classification in construction sites,” in *EUSIPCO*, 2021, pp. 810–814.
- [13] Y. Gong, Y.-A. Chung, and J. Glass, “AST: Audio Spectrogram Transformer,” in *Interspeech*, 2021, pp. 571–575.
- [14] C. Drioli and D. Rocchesso, “Learning pseudo-physical models for sound synthesis and transformation,” in *IEEE SMC*, 1998, pp. 1085–1090.

- [15] A. Uncini, “Sound synthesis by flexible activation function recurrent neural networks,” in *13th Italian Workshop on Neural Nets*, 2002, pp. 168–177.
- [16] K. Itoyama and H. G. Okuno, “Parameter estimation of virtual musical instrument synthesizers,” in *ICMC*, 2014.
- [17] H. Zhou, F. Yu, and X. Wu, “Audio mixing inversion via embodied self-supervised learning,” *Machine Intelligence Research*, pp. 55–62, 2024.
- [18] C. Peladeau and G. Peeters, “Blind estimation of audio effects using an auto-encoder approach and differentiable digital signal processing,” in *IEEE ICASSP*, 2024, pp. 856–860.
- [19] J. Koo, S. Paik, and K. Lee, “End-to-end music remastering system using self-supervised and adversarial training,” in *IEEE ICASSP*, 2022, pp. 4608–4612.
- [20] R. M. Bittner, J. Salamon, M. Tierney, M. Mauch, C. Cannam, and J. P. Bello, “Medleydb: A multitrack dataset for annotation-intensive mir research,” in *ISMIR*, 2014, pp. 155–160.
- [21] D. Tardieu, E. Detruy, and G. Peeters, “Production effect: Audio features for recordings techniques description and decade prediction,” in *DAFx*, Sep. 2011, pp. 441–446.
- [22] M. Huzaifah, “Comparison of time-frequency representations for environmental sound classification using convolutional neural networks,” *arXiv preprint arXiv:1706.07156*, 2017.
- [23] B. McFee, C. Raffel, D. Liang, D. P. Ellis, M. McVicar, E. Battenberg, and O. Nieto, “librosa: Audio and music signal analysis in python,” in *SciPy*, 2015, pp. 18–24.
- [24] A. Défossez, N. Usunier, L. Bottou, and F. Bach, “Music source separation in the waveform domain,” *arXiv preprint arXiv:1911.13254*, 2019.
- [25] J. Imort, G. Fabbro, M. A. M. Ramírez, S. Uhlich, Y. Koyama, and Y. Mitsu-fuji, “Removing distortion effects in music using deep neural networks,” *arXiv preprint arXiv:2202.01664*, 2022.
- [26] D. Fourer and G. Peeters, “Objective characterization of audio signal quality: applications to music collection description,” in *IEEE ICASSP*, 2017, pp. 711–715.